SINTEF
PROCEEDINGS
2

Proceedings of the 12th International Conference on Computational Fluid Dynamics in the Oil & Gas, Metallurgical and Process Industries

Progress in Applied CFD – CFD2017

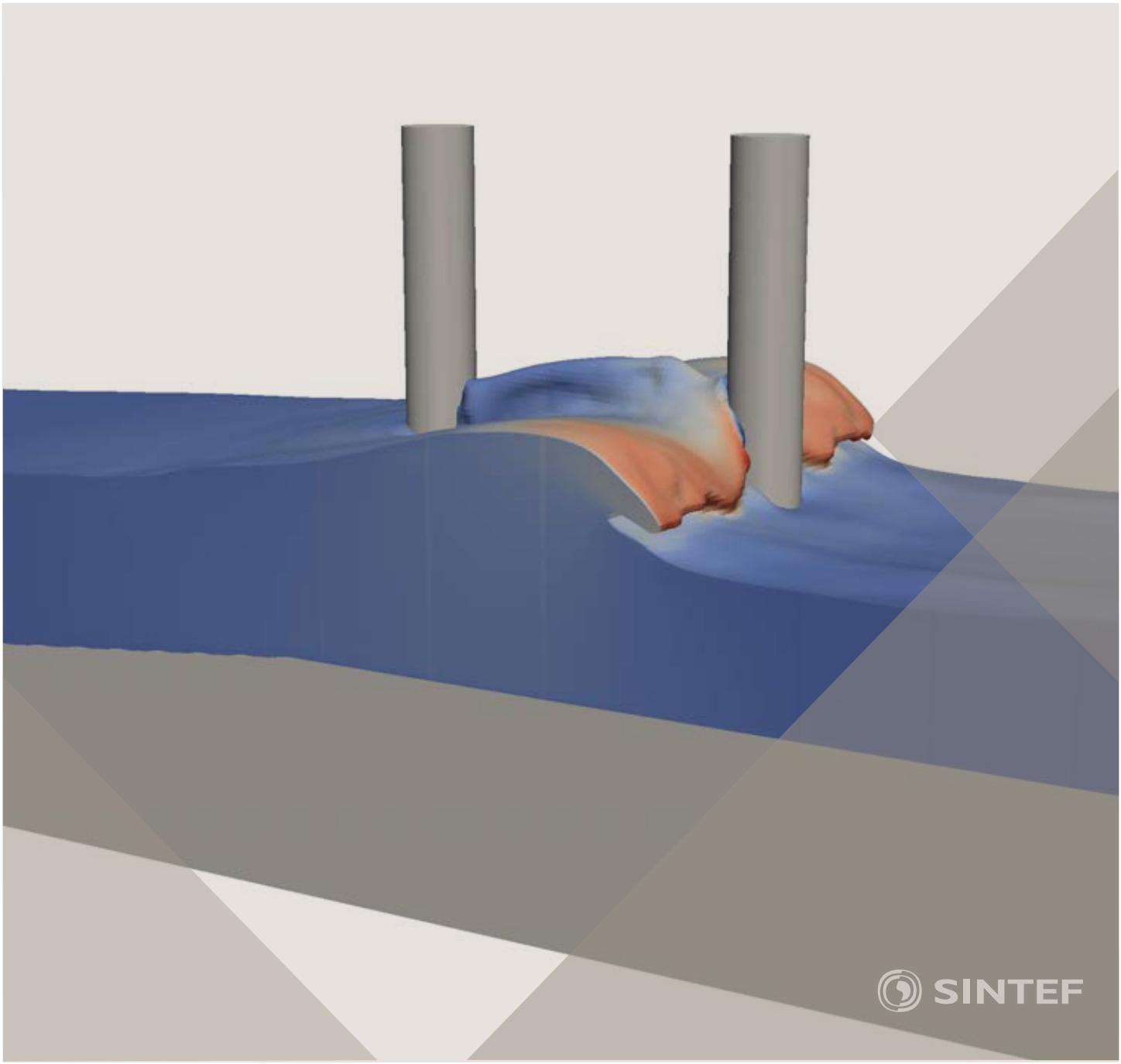

SINTEF Proceedings

Editors:
Jan Erik Olsen and Stein Tore Johansen

Progress in Applied CFD – CFD2017

Proceedings of the 12th International Conference on Computational Fluid Dynamics in the Oil & Gas, Metallurgical and Process Industries

SINTEF Academic Press

SINTEF Proceedings no 2
Editors: Jan Erik Olsen and Stein Tore Johansen
Progress in Applied CFD – CFD2017
Selected papers from 10th International Conference on Computational Fluid Dynamics in the Oil & Gas, Metallurgical and Process Industries

Key words:
CFD, Flow, Modelling

Cover, illustration: Arun Kamath

ISSN 2387-4295 (online)
ISBN 978-82-536-1544-8 (pdf)

SINTEF Academic Press
Address: Forskningsveien 3 B
PO Box 124 Blindern
N-0314 OSLO
Tel: +47 73 59 30 00
Fax: +47 22 96 55 08

www.sintef.no/byggforsk
www.sintefbok.no

SINTEF Proceedings
SINTEF Proceedings is a serial publication for peer-reviewed conference proceedings on a variety of scientific topics.
The processes of peer-reviewing of papers published in SINTEF Proceedings are administered by the conference organizers and proceedings editors. Detailed procedures will vary according to custom and practice in each scientific community.

PREFACE

This book contains all manuscripts approved by the reviewers and the organizing committee of the 12th International Conference on Computational Fluid Dynamics in the Oil & Gas, Metallurgical and Process Industries. The conference was hosted by SINTEF in Trondheim in May/June 2017 and is also known as CFD2017 for short. The conference series was initiated by CSIRO and Phil Schwarz in 1997. So far the conference has been alternating between CSIRO in Melbourne and SINTEF in Trondheim. The conferences focuses on the application of CFD in the oil and gas industries, metal production, mineral processing, power generation, chemicals and other process industries. In addition pragmatic modelling concepts and bio-mechanical applications have become an important part of the conference. The papers in this book demonstrate the current progress in applied CFD.

The conference papers undergo a review process involving two experts. Only papers accepted by the reviewers are included in the proceedings. 108 contributions were presented at the conference together with six keynote presentations. A majority of these contributions are presented by their manuscript in this collection (a few were granted to present without an accompanying manuscript).

The organizing committee would like to thank everyone who has helped with review of manuscripts, all those who helped to promote the conference and all authors who have submitted scientific contributions. We are also grateful for the support from the conference sponsors: ANSYS, SFI Metal Production and NanoSim.

Stein Tore Johansen & Jan Erik Olsen

Organizing committee:

Conference chairman: Prof. Stein Tore Johansen
Conference coordinator: Dr. Jan Erik Olsen
Dr. Bernhard Müller
Dr.Sigrid Karstad Dahl
Dr.Shahriar Amini
Dr.Ernst Meese
Dr.Josip Zoric
Dr.Jannike Solsvik
Dr.Peter Witt

Scientific committee:

Stein Tore Johansen, SINTEF/NTNU
Bernhard Müller, NTNU
Phil Schwarz, CSIRO
Akio Tomiyama, Kobe University
Hans Kuipers, Eindhoven University of Technology
Jinghai Li, Chinese Academy of Science
Markus Braun, Ansys
Simon Lo, CD-adapco
Patrick Segers, Universiteit Gent
Jiyuan Tu, RMIT
Jos Derksen, University of Aberdeen
Dmitry Eskin, Schlumberger-Doll Research
Pär Jönsson, KTH
Stefan Pirker, Johannes Kepler University
Josip Zoric, SINTEF

CONTENTS

CFD EROSION MODELING OF BLIND TEES

Arnaud SANCHIS*, Alexander SKORGEN
TechnipFMC, Philip Pedersens vei 7, 1366 Lysaker, NORWAY
* E-mail: arnaud.sanchis@technipfmc.com

ABSTRACT

In subsea components such as Production Trees (XT) where the production flow path is machined out of steel blocks, the flow changes direction abruptly at blind tees or sharp elbows, causing increased erosion risks compared to a piping design. The risk of erosion is largely controlled by the depth of the cavity inside a flow-turning element, which may vary between zero for a sharp elbow and more than one time the Inner Diameter (ID) for a full blind tee. In this paper, a comparison between the erosion response of three different flow-turning elements is performed by using Computational Fluid Dynamics (CFD) with transient particle tracking: a blind tee with a deep cavity, a blind tee with a shallow cavity (depth < 1 ID) and a sharp elbow. The DNVGL-RP-O501 (2015) erosion response model is implemented in the simulations with a modification to the angle function which aims at filtering out erosion results due to impacts at low angle. The transient formulation causes the sand particles to be dispersed naturally by the flow field, yielding time-averaged realistic erosion results without any need for area-averaging or numerical dispersion schemes. The CFD model is successfully benchmarked against the DNVGL-RP-O501 (2015) guidelines for standard piping components such as bends.

The simulation results reveal that the shallow cavity blind tee creates a very high risk of erosion inside the cavity which is not predicted by the guidelines, with peak erosion rates one order of magnitude higher than for a sharp elbow. This is observed both for a gas and liquid production case, and a physical explanation for this behaviour is provided based on an analysis of the transient flow and sand particle dynamics. Although further numerical sensitivities and experimental evidence are required to confirm this result, it is advised to avoid blind tees with a shallow cavity (less than one time the inner diameter of the flow path) for designing subsea production systems where sand production can be expected.

Keywords: Erosion, CFD, SPS design

NOMENCLATURE

Greek Symbols

α	Impact angle, [rad]
ρ_{MAT}	Wall material density [kg/m^3]

Latin Symbols

A_{IMPACT}	Area of impact [m^2]
CFD	Computational Fluid Dynamics
DPM	Discrete Phase Modeling
E_{MF}	Erosion mass flux, [kg/m^2]
E_{RATE}	Erosion rate, [mm/year]
E_{RATIO}	Erosion ratio, [kg/kg]
f	Impact angle function
GF	Geometry Factor
ID	Inner Diameter, [mm]
k	Material coefficient, [-]
$\dot{m}$	Sand mass rate, [kg/s]
SPS	Subsea Production System
V_p	Particle velocity, [m/s]
XT	Production tree

INTRODUCTION

Solid particles consisting of sand, gravel or proppants may be produced from subsea wells for certain conditions related to rock formation stability, well completion design and production parameters such as flow rate or bottom hole pressure. As they pass through the Subsea Production System (SPS), solid particles impact on the inner walls of equipment conveying the flow of hydrocarbons to topside, causing over time loss of material. This phenomenon is generally described as "erosion" and, if not managed properly, may have serious consequences for the integrity and functionality of the SPS.

The prediction of material loss caused by erosion over life of the field is one of the key competence area within the Flow Assurance discipline at TechnipFMC. Erosion analysis relies on two different tools: screening calculations, which are based on empirical models applicable to standard types of components, and detailed calculations based on Computational Fluid Dynamics (CFD) which solve the equation of motion for the flow and solid particles within a 3D geometry of the SPS.

Erosion response model

Both screening and detailed erosion calculation use a wall response model, which determines the amount of material removed from the wall at particle impact as a function of the mass, impact angle and impact velocity of the particle. The erosion ratio E_R is expressed in kg of material removed per kg of incoming particle and takes the form

$$E_{RATIO} = k \times V_p^n \times f(\alpha) \qquad (1)$$

In Equation (1), the velocity exponent n, material constant k and the angle function $f(\alpha)$ vary depending on the model employed. This study is based on the erosion

response model from DNVGL-RP-O501 (2015). Multiplying E_R by the mass flow rate of incoming sand and dividing by the density of inner wall material and area of impact, the thickness of material lost per unit of time (erosion rate) is obtained:

$$E_{RATE} = E_{RATIO} \cdot \dot{m} / \rho_{MAT} \cdot A_{IMPACT} \quad (2)$$

Erosion rates are usually expressed in mm/year, and cumulated over several years of production to calculate the total erosion wear over life of the field. The erosion wear is finally compared to the allowance, i.e. the thickness of material which may be eroded without compromising the integrity or functionality of the equipment.

Erosion screening calculations

DNVGL-RP-O501 (2015) contains empirical models applicable to standard components such as reducers, bends or blind tees which are typical "hot-spots" for erosion in a SPS. Based on the component's dimensions, solid and fluid (carrier) phase properties and production parameters, an erosion rate is provided from a simple model validated by experimental data.

These empirical models may easily be implemented in a spreadsheet or script and applied to large datasets of production cases for early risk screening and sensitivity purposes. However, they rely on important assumptions which may limit their applicability for certain geometries and / or flow conditions:

1. The sand particles are considered uniformly distributed across the flow area upstream of the component
2. A single fluid phase (with mixed properties based on volume fraction average for multiphase flows) is considered with a uniform velocity profile upstream of the component
3. The erosion rate is predicted for a single hot-spot per component corresponding to the main impact area of sand particles
4. The geometry of the component evaluated should be similar to the samples tested experimentally to validate the empirical models.

An example is provided in Figure 1 for a component referred to as “blind tee” in DNVGL-RP-O501 (2015). The geometry shown represents one of the samples tested at DNVGL. The cavity depth is 50 mm, more than the Inner Diameter (ID) of the inlet flow cross-section. The hot-spot considered in the empirical model corresponds to an impact area situated at the extrados outlet wall. Uniform flow conditions and sand particle concentration are assumed in the vertical inlet upstream of the tee.

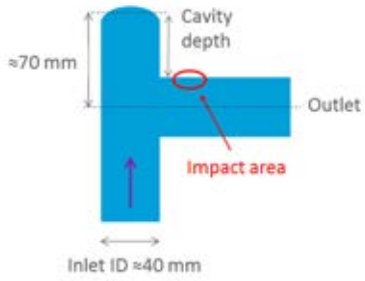

Figure 1: Example of blind tee experimental geometry tested at DNVGL (courtesy of DNVGL).

Erosion detailed calculations based on CFD

Erosion CFD computations combine two simulation processes, performed either sequentially (steady-state models) or simultaneously (transient models):

- The simulation of the carrier flow in the system consisting of one or several fluid phases, using an Eulerian approach
- The simulation of the sand particles (solid phase) using a Lagrangian approach whereby individual particles are tracked in space (steady-state models) or time and space (transient models).

The number of individual sand particles tracked in one simulation is in the range of 50 000 to several millions in order to yield statistically representative results. Each time a sand particle impacts a wall boundary and rebounds into the domain, the erosion model from Equation (1) is used to compute the mass of material removed from the wall. The greatest potential added value of the CFD approach compared to screening calculations is that no assumption on the sand distribution and flow profile upstream of a component is needed as long as the upstream extent of the computational domain is sufficient. Also, CFD simulations consider the actual geometry of the SPS and should be used when assessing erosion on components for which no empirical screening model is available.

Geometry Factors (GF)

Geometry Factors (GF) have been introduced in DNVGL-RP-O501 (2015) to account for the effect of the upstream flow path layout on erosion results. These factors are directly applied to the empirical models used for screening calculations and may vary between 1 and 4:

$$E_{RATE-CORR} = GF \cdot E_{RATE} \quad (3)$$

A value of 1 is used if the component of interest is placed downstream a long straight section of piping so that the flow and sand concentration profile can be considered as uniform. A value of 4 corresponds to a case where multiple flow-turning elements are present upstream of the component with the flow path in several planes. This induces a swirl component in the flow that contributes to focusing the sand particles and creating enhanced erosion locally.

Geometry Factors may also be directly obtained from CFD simulations by dividing the simulated erosion rate by the result from an empirical model, provided that the

extent of the computational model is sufficient to capture all relevant upstream effects.

Based on TechnipFMC's experience, the GF values specified in DNVGL-RP-O501 (2015) are retrieved when comparing CFD and screening results for most of the hot-spots encountered in an SPS erosion analysis, i.e. values in the range of 1 to 4 are usually obtained. However, in subsea components such as Production Trees (XT) where the production flow path is machined out of steel blocks, the Geometry Factors are sometimes found to be much larger, as illustrated in the following.

Application of screening and CFD erosion calculations for SPS design

The flowpath in a SPS from the well tubing to the flowline consists of a succession of flow-turning elements (bends, elbows, blind tees) and ID variations separated by straight sections. In Figure 2, erosion contours from a detailed CFD erosion analysis on part of a SPS are displayed. A single phase, transient simulation with particle tracking has been run with a total of 15 million particles injected into the domain. Twelve erosion hot-spots have been identified at locations which could not always be predicted by the screening empirical models (for example, hot-spot 3 in Figure 2 upstream of the second elbow). The elbow geometry itself is not described in DNVGL-RP-O501 (2015), where the only flow-turning elements considered consist of bends or blind tees.

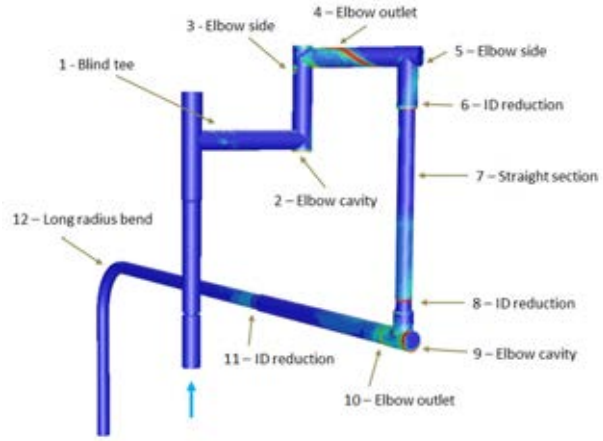

Figure 2: Example of SPS flowpath and erosion results.

Figure 3 shows the instantaneous location of the sand particles in the domain and their velocity. Upstream of the first blind tee, which is preceded by a long vertical section corresponding to the well tubing, the sand particles are homogeneously distributed across the inner bore cross-section. However, the close succession of flow-turning elements in multiple planes distorts the velocity profile and introduces a swirl component which tends to focus the sand particles. It is obvious that downstream of the second elbow, the assumption of homogeneous sand concentration is no longer valid.

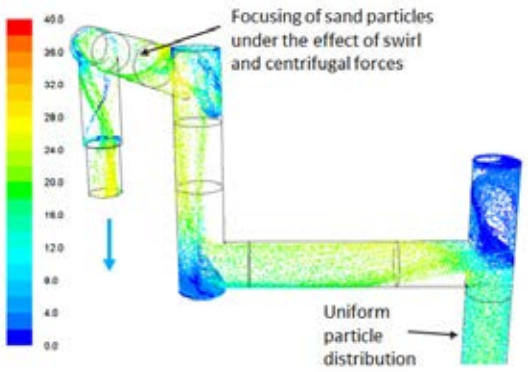

Figure 3: Instantaneous sand particle tracks coloured by velocity magnitude (m/s).

A comparison of CFD erosion results to screening calculations indicates that Geometry Factors are in the range of 0.3 to 3.4 for most of the hot-spots shown in Figure 2. However, much higher values are obtained for some components. In Figure 4, CFD erosion results at the outlet of two elbows corresponding to hot-spots 4 and 10 in Figure 2 are shown. Both flow-turning elements have similar inlet ID and geometry. The application of DNVGL-RP-O501 (2015) to these elbows, represented as a bend with a radius of 0.5 ID and a Geometry Factor of 1, yields an erosion rate of 0.02 mm/year. Hot-spot 10 is situated downstream a long vertical section of piping which allows the flow profile and sand concentration to recover before entering the elbow. The CFD results obtained at the outlet confirm the erosion rate from the screening methodology with GF of 1. On the contrary, hot-spot 4 is situated downstream three flow-turning elements (one blind tee and two elbows), in different planes and separated by 4 to 6 IDs only. The erosion rate is 0.5 mm/year, corresponding to a Geometry Factor of 25 (0.5 / 0.02). The configuration upstream of hot-spot 4 is representative of designs where the flow path is machined out of steel blocks. This reduces the streamwise separation between flow-turning elements and replaces pipe bends or blind tees with sharp elbows, creating added distorsion of the flow velocity profile and focusing of sand particles compared to a piping design.

Some care and engineering judgement should be used when applying Geometry Factors from CFD results to the screening of SPS designs. However, such information may be used to provide useful feedback to designers: adding an inline cavity with a depth > 1 ID to the elbow situated upstream of hot-spot 4 may reduce the Geometry Factor for hot-spot 4, for example.

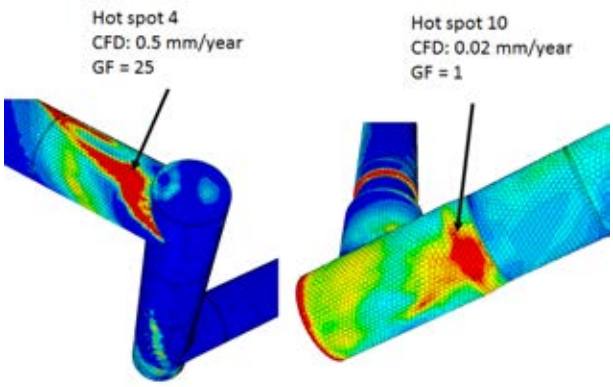

Figure 4: Comparison of CFD to screening results at the outlet of two elbows with different upstream flow configuration.

CASE EXAMPLE: EROSION IN BLIND TEES

In the following, the effect of the cavity depth on the erosion performance of a blind tee is investigated using the same approach as described previously. The purpose of this work is to compare erosion results for actual flow-turning element geometries to the results provided by the DNVGL-RP-O501 (2015) empirical models.

Blind tee cavity depth

There is ample experimental and numerical evidence that blind tees have a dampening effect on erosion compared to sharp bends. Due to the local increase of the inner cross-section as the flow changes direction, the fluid and sand particle velocity at the outlet of a blind tee are lower than for a 90 degrees, short radius bend. In addition, at least part of the sand particles penetrate the low-velocity, high pressure zone inside the cavity where they lose momentum and recirculate instead of impacting the wall at the extrados outlet. Both of those effects are illustrated in Figure 13 by comparing particle trajectories and velocity for the "full" blind tee (top) and the sharp elbow (bottom). For more insight on particle dynamics inside bends and blind tees, reference is made to Chen (2004).
This behaviour is captured in the empirical models of DNVGL-RP-O501 (2015): for gas flow conditions and small particle diameters, the erosion rate for a blind tee is about 5 times lower than for a short radius bend of similar ID. DNVGL-RP-O501 (2015) does not contain any definition of the geometrical characteristics of a blind tee. Presumably, it is assumed that the term "blind tee" refers to a standard piece of equipment which corresponds to the sketch provided in Figure 1, where the cavity depth is large enough to provide the benefits described above in terms of erosion performance. However, tees machined out of steel blocks may have cavities deeper or shallower than presented in Figure 1, depending on the drilling length for each perpendicular section of the flow path. Therefore, there is an uncertainty regarding the minimum cavity depth that such a component should have to qualify as a "blind tee" according to DNVGL-RP-O501 (2015).

Model set-up

Softwares and hardware used
The work reported here has been performed using the following softwares:

- BETA ANSA version 16 for pre-processing (geometry and mesh generation)
- ANSYS Fluent version 17.1 for solving and post-processing.

All simulations have been run on a 128 cores cluster and have required approximately one day of computational time for each case. The cluster consists of 4th generation Xeon E5 CPUs with 32 GB RAM, interconnected with Infiniband at 56 Gb/s.

Geometry
The geometries investigated are shown in Figure 5. The flow-turning element is preceded by a 13 ID section of straight piping. A square-step contraction equal to 50% of the cross-sectional area is placed 10 ID upstream of the tee to trigger transient effects in the flow and enhance the dispersion of sand particles upstream of the tee. The particle injection plane is placed 6 ID upstream of the tee. Three different flow-turning elements have been investigated:

1. A "full" blind tee with a cavity depth equal to the inlet ID
2. A "shallow" blind tee with a cavity depth equal to 38% of the inlet ID
3. A sharp elbow (i.e. a blind tee with cavity depth reduced to zero).

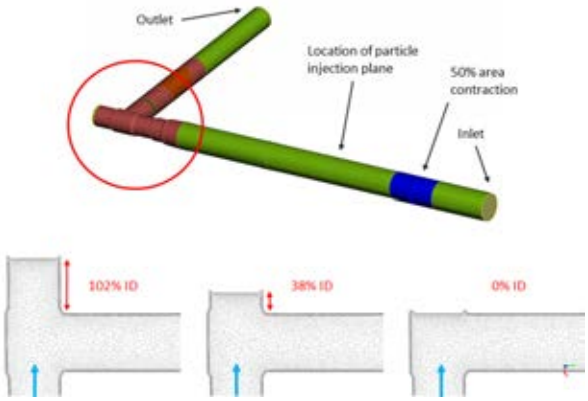

Figure 5: Geometries investigated in blind tee erosion CFD study

Production cases
Two production cases have been simulated which aim to represent typical gas and liquid production from a subsea well through a 5-inch (≈130 mm ID) XT. Production parameters are listed in Table 1. The fluid is considered as single phase. In this work, the solid particles in the flow are assumed to be sand grains with a density of 2650 kg/m^3 and uniform size. All surfaces of impact consist of Inconel with a density of 8440 kg/m^3.

Table 1: Production cases simulated

	Gas case	Liquid case
Fluid mass flow rate	40.0 kg/s	85.8 kg/s
Fluid bulk velocity upstream of tee	32.9 m/s	8.1 m/s
Fluid density	110 kg/m^3	961 kg/m^3
Fluid viscosity	0.017 cP	0.696 cP
Sand mass flow rate	0.074 g/s	0.858 g/s
Sand particle size	50 µm	250 µm

Transient methodology

The computational model used in this study relies on the simultaneous solution of the fluid and sand particle equations of motion with a time-dependent (i.e. transient) approach. At each time step in the simulation, the flow field and position of the particles are computed. Erosion wear accumulates over time and is monitored at the different hot-spots in the model. The simulation is run until sufficient statistics are accumulated to calculate a rate of erosion in mm/year.

The transient approach yields results which are much more realistic than the "steady-state" approach, whereby the motion of the sand particles is solved onto a frozen flow field. It is especially recommended for designs such as presented in Figure 2 and Figure 5 where the flow-turning elements consist of sharp elbows rather than smooth pipe bends. Downstream of each elbow, the flow separates from the wall and forms large-scale turbulent vortices which are conveyed downstream to the next flow-turning element. Sand particles will tend to coalesce into "packets" or narrow bands under the effect of swirl, recirculation and vortex shedding. This is illustrated in Figure 6, where snapshots of the sand particle concentration in the domain at two different instants are shown.

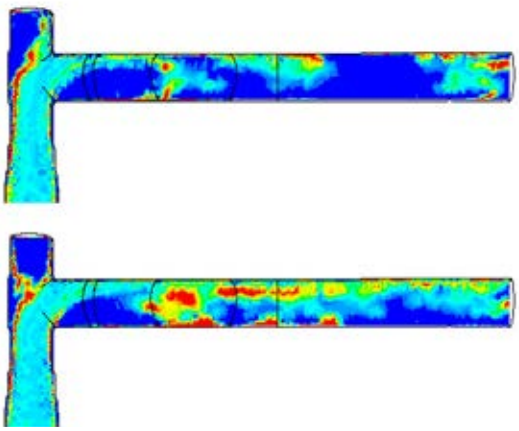

Figure 6: Contours of sand particle concentration at two different instants in the simulation (full blind tee, gas production case).

The instantaneous rate of erosion at any location may vary considerably with time, as illustrated in Figure 7 for the case of an intrusive erosion probe. The total simulation time should therefore be much larger than the time scale of the flow and particle dynamics, so that a linear rate of erosion can be calculated. Reference is made to Equation (4) for the relation between the erosion rate and erosion mass flux.

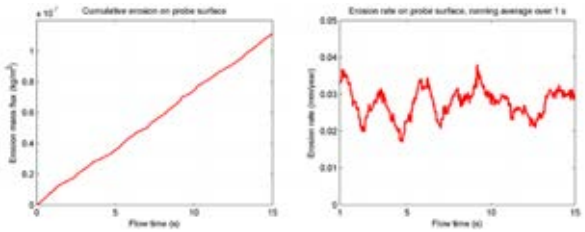

Figure 7: Transient CFD erosion results: increase of erosion mass flux (kg/m^2) with simulation time on an erosion probe placed in the flow path (left), and instantaneous erosion rate (mm/year) calculated based on 1 s running average (right)

Fluid and discrete phase modelling

The continuous fluid phase is modelled as incompressible. Turbulence effects are resolved using a k-ω SST model with automatic wall treatment, because the constraints placed on the mesh aspect ratio do not allow to use a low y^+ approach, especially for the gas phase. The time step in the simulation is set to obtain a Courant number below 5.

Fluent's Discrete Phase Modeling (DPM) approach is used to model the sand particles and their interaction with the fluid. In DPM, particles are modeled as point masses with no physical volume, an assumption which is valid as long as the effect of collisions between particles is negligible. Sommerfeld (2016) indicates that particle-particle interactions become important for sand volume fractions above 0.001, which is several orders of magnitude above the value for this case.

Numerical "parcels" representing sand particles are injected at each time step from a plane situated 6 ID upstream of the tee, and consisting of 648 points distributed as a grid across the flow cross-section (Figure 8). The parcels are subject to inertial, gravity and drag forces only. Given the high Reynolds number and low Stokes relaxation times, turbulent dispersion may play an important role. For steady-state erosion CFD analyses, turbulent dispersion must be accounted for because it is the only term which causes dispersion of sand particles in the domain. However, in the present case, it is assumed that the effects of turbulent dispersion are inherently captured by the transient simulation procedure, whereby parcels are tracked in the domain with the same time step as the flow solution. A two-way fluid coupling approach is used.

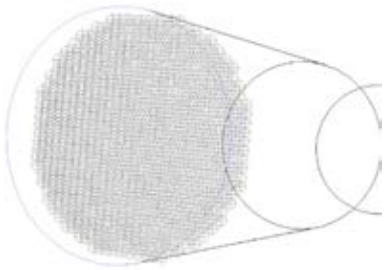

Figure 8: Sand particle injection locations

Erosion wall response model

The erosion response model from DNVGL-RP-O501 (2015) has been implemented as a boundary condition at all walls in the domain by entering the parameters

introduced in Equation (1). For every impact of a sand particle with the walls, the following computational steps are performed:

- The particle rebounds into the domain (energy restitution coefficients of 0.8 and 1.0 are used in the normal and tangential directions, respectively)
- The mass of metal lost at the cell where the impact occurs is calculated according to Equation (1).

The mass of metal lost is normalized by the cell surface to compute an erosion mass flux expressed in kg of metal removed per unit area of wall. This value increases monotonically with simulation time in each cell as more sand particles collide with the wall.

The model from DNVGL-RP-O501 (2015) is modified by setting the angle function to zero for all impact angles less than 5° (see Figure 9). This correction has been implemented based on numerous observations of high erosion predicted by CFD in areas of flow recirculation with low particle density and / or low velocities such as cavities, dead legs or separation bubbles. For numerical reasons which have not yet been clarified, the presence of sand particles at those locations (not directly impacting but rather "brushing" along the wall) produces significant, unphysical erosion results. The DNVGL-RP-O501 (2015) erosion response model only applies to particle impacts with high enough angle, at which the sand grains "cut" through the metal. Therefore, it is considered that applying a cut-off angle to the function f in Equation (1) is a valid approach to filter out unphysical erosion results from the simulations.

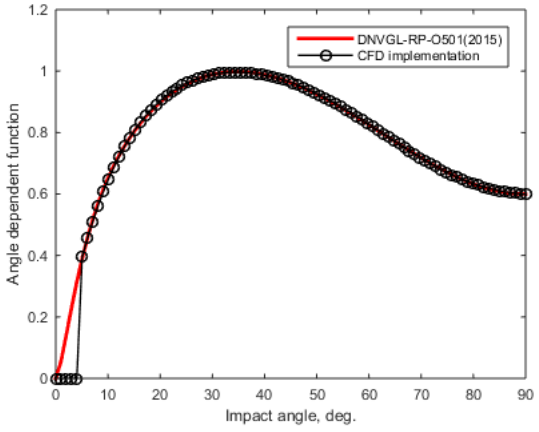

Figure 9: Angle function implemented in CFD simulations

Sensitivities have been performed to ensure that the erosion rate in areas of direct particle impact is not affected by this modification. An example is provided in Figure 10: the erosion rate at the intrados of the blind tee has been reduced by a factor of 3 with the application of the cut-off angle, whereas the erosion rate at the extrados is unchanged.

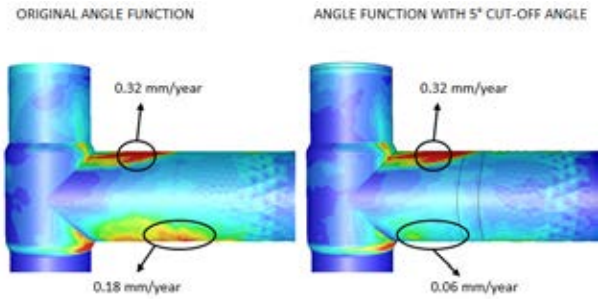

Figure 10: Effect of cut-off angle on erosion results for a blind tee. Gas production case with 250 µm particles.

Mesh design

The same mesh is used to resolve the Eulerian fluid motion and the Lagrangian particle trajectories, and is applied to both production cases listed in Table 1. The mesh was first designed as an unstructured grid with tetrahedral elements and prisms in the inflation layers, then converted to polyhedral elements. The thickness of the first inflation layer is 150 µm and the quality metrics are listed in Table 2.

Table 2: Mesh parameters and quality metrics

Element type	Polyhedrals (prisms in inflation layers)
Number of cells	1.1 million
First layer thickness	150 µm
Element base size	7 mm (5% of ID)
Minimum orthogonal quality	0.11
Maximum equiangle skewness	0.87
Maximum aspect ratio	154

In DNVGL-RP-O501 (2015), it is recommended that the first layer thickness of the mesh on which the particle trajectories are solved should be 3 to 5 times larger than the sand particle diameter. In the present study, this criterion is met for the gas production case, but not for the liquid production case with 250 µm particles. However, sensitivities have been performed on the first layer thickness and showed that with the numerical setup used, no variations in the erosion results were observed with first layer thickness varying between 5 and 0.4 times the particle size. Unphysical erosion results have been observed in cells with a high aspect ratio, though. Therefore, attention has been given in the mesh design to the orthogonal quality and aspect ratio, rather than the ratio between the first layer thickness and the sand particle size.

Results

The simulations for the gas and liquid production cases have been conducted in three steps:

1. The transient flow solution is computed without sand particles, until stationary velocity fluctuations are obtained downstream of the tee
2. Particles are injected at each time step and progressively fill the domain. The total mass of sand in the domain is monitored: when steady state conditions are reached, the erosion mass flux at the walls is monitored

3. The simulation is stopped when a constant erosion rate has been calculated at each hot-spot from the erosion mass flux values monitored:

$$E_{RATE} = \partial / \partial t \; E_{MF} \times \frac{1}{\rho_{MAT}} \qquad (4)$$

It is important to note that all erosion mass fluxes used to compute erosion rates are maximum values over all vertices forming the "hot-spot", i.e. no area-averaging of results is performed (Figure 11). Such post-processing techniques are often necessary in steady-state simulations to account for the lack of dispersion in the sand particle impacts. TechnipFMC's practice is to area-average all steady-state erosion results over a circular surface equal to 10% of the pipe ID as suggested in DNVGL-RP-O501 (2015) and described in Leong (2016). In the present case, impact points vary in time due to the dynamics of the flow and sand particles, so that no post-treatment of the erosion results is required.

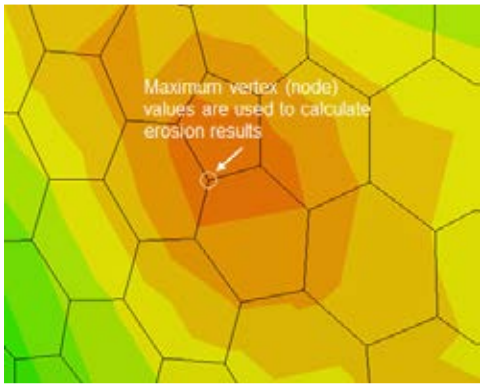

Figure 11: Example of erosion mass flux contours at one hot-spot

Approximately 10 seconds of flow time have been simulated for each production case, with a time step of 0.1 milliseconds for the gas production case and 0.5 milliseconds for the liquid case. The corresponding total number of parcels tracked in the simulation is around 60 million and 12 million, respectively.

Sand mass in the domain

The evolution of the sand mass present in the computational domain with simulation time is presented in Figure 12. Particle are injected at t = 1 s and progressively fill up the domain until a steady-state regime is established for the sand load. This indicates that the time-averaged mass of sand in the domain is constant, i.e. there is no accumulation of sand. A lower value is obtained for the sharp elbow than for the full blind tee since the volume of fluid in the domain is smaller. Important fluctuations of the sand load are obtained for the shallow tee geometry, especially for the liquid case. This is due to the periodic accumulation and release of sand particles in the shallow cavity.

There were no incomplete particle path in the simulation, meaning that all particles injected exited the domain at the outlet.

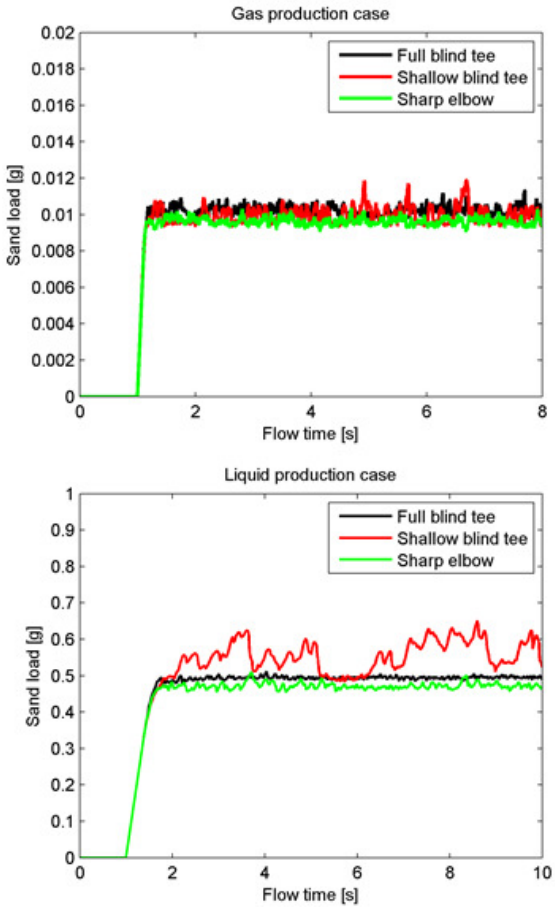

Figure 12: Time evolution of sand mass in the domain. Top: gas production case, bottom: liquid production case

Particle tracks

In Figure 13, tracks of the sand particles at one instant in the simulation are shown, coloured by velocity magnitude and residence time, for the liquid production case. Similar results are obtained for the gas production case.

As the cavity depth is reduced, the maximum velocity of the particles downstream of the flow-turning element increases because the flow cross-sectional area is smaller. The particle tracks for the shallow blind tee indicate the presence of a strong vortex cell inside the cavity which entrains particles with quite high velocity. This is confirmed by the flow velocity and vorticity results plotted in Figure 14: the vortex is much weaker for the full blind tee, and almost disappears for the sharp elbow. An analysis of the animations of the particle tracks over the full simulation time allows to link observations made from Figure 12, Figure 13 and Figure 14. The vortex cell inside the shallow blind tee cavity is unstable: as it grows in strength, a large number of sand particles are entrained inside the cavity and recirculate with high velocity. They are projected against the back wall of the cavity, creating important erosion at this location. Then, with a periodicity which is visible in the sand loading plot in Figure 12, the vortex collapses and all sand particles are released in the flow. This behaviour is unique to the shallow blind tee: inside the full blind tee, the flow of sand particles into and out of the cavity is almost steady and velocities are low. For the sharp elbow, the cavity is reduced to the upper back corner of the elbow, and this volume does not appear to be large enough to sustain the

same flow mechanism as observed for the shallow blind tee.

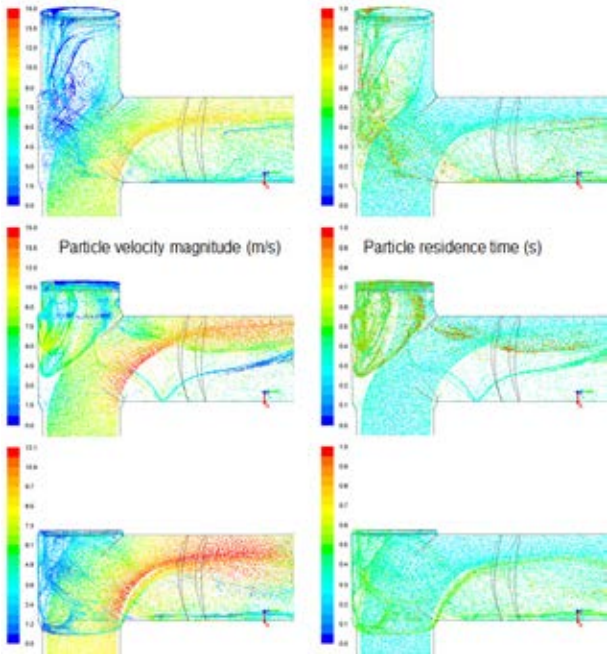

Figure 13: Particle tracks coloured by velocity magnitude (left) and residence time (right), liquid production case, for the three geometries investigated

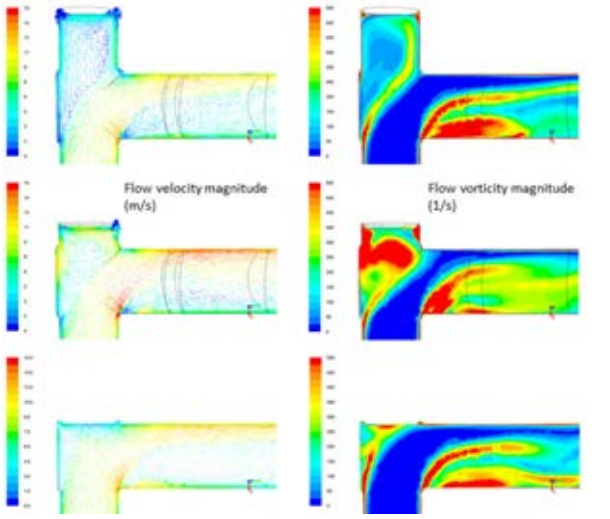

Figure 14: Flow velocity vectors coloured by velocity magnitude (left) and vorticity contours (right), liquid production case, for the three geometries investigated.

Erosion results

Contours of the erosion mass flux at simulation end are displayed in Figure 15. For each geometry and each production case, the maximum erosion rate obtained over the whole geometry is listed in Table 3 and compared to the screening result from the application of DNVGL-RP-O501 (2015). The "blind tee" empirical model has been used for the full blind tee geometry, and the "bend" model with a radius of 0.5 ID has been used for the shallow blind tee and sharp elbow geometries. A Geometry Factor of 1 has been considered for the screening calculations, since the upstream flow path only consists of a straight, vertical section.

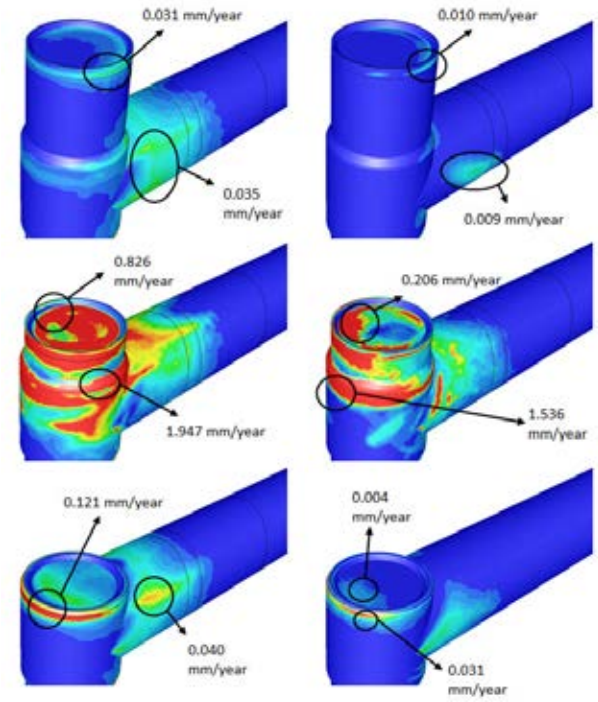

Figure 15: Contours of erosion mass flux at simulation end and erosion rates at hot-spots for the three geometries investigated. Left: gas production case, right: liquid production case. Different scaling is used for the two production cases.

Table 3: Comparison of CFD results to screening results

Geometry	DNVGL-RP-O501 model (GF = 1)	Prod. case	Screening result (mm/year)	CFD result (mm/year)	Geometry Factor (CFD / screening)
Full blind tee	Blind tee	Gas	0.028	0.035	1.2
		Liquid	0.004	0.010	2.5
Shallow blind tee	0.5 ID radius bend	Gas	0.154	1.947	12.6
		Liquid	0.024	1.536	64.0
Sharp elbow	0.5 ID radius bend	Gas	0.154	0.121	0.8
		Liquid	0.024	0.031	1.3

A massive increase in the erosion rate is observed for the shallow blind tee, both for the gas and liquid production cases. The maximum erosion rate is increased by one order of magnitude when comparing results between the full and shallow blind tees. The most severe erosion is reported at the cavity back wall, and is caused by the presence of the unstable vortex cell described earlier. When reducing the cavity depth down to zero (sharp elbow), erosion rates drop back to expected values for a sharp flow-turning element.

The comparison of the CFD and screening results shows that the full blind tee and sharp elbow may be described using the "blind tee" and "0.5 ID bend radius" models. Proportionality factors between the CFD and screening results are comprised between 0.8 and 2.5. However, factors of 12.6 and 64.0 are obtained from the CFD results for the shallow blind tee, indicating that the erosion performance of such geometries may be much worse than either a "blind tee" or a "sharp elbow".

Limitations and uncertainty

The erosion results obtained inside the blind tee with shallow cavity are caused by a large-scale instability in the flow. The representation of this flow structure in CFD is subject to large uncertainties due to limitations of the turbulence modeling, insufficient discretization of near-wall regions and other numerical effects. It is therefore recommended to perform further sensitivities to confirm this result, particularly related to the mesh density and turbulence model employed.

Another important source of uncertainty is the assumption of single phase flow which has been taken to represent the flow. Virtually all production streams contain both a liquid and gas phase at subsea conditions. Multiphase flow effects on erosion CFD simulations have been briefly discussed in Leong (2016) and may be significant in the present case: in a gas production case, liquid will most likely accumulate inside the tee cavity and may have a "cushioning" effect on erosion. The presence of a second fluid phase may also affect the unstable vortex structure which creates the present results for the shallow blind tee.

CONCLUSIONS

The geometry of blind tees inside SPS parts which are machined out of steel blocks may deviate from standardized flow-turning elements found in piping designs. In particular, the depth of the blind tee cavity may vary between zero (sharp elbow) and more than one time the ID. In this paper, the impact of the cavity depth on the erosion performance of such blind tees has been assessed by considering three geometries with cavity depth of 1 ID ("full" blind tee), 0.38 ID ("shallow" blind tee) and 0 ID (no cavity, i.e. sharp elbow).

Results are compared to the DNVGL-RP-O501 (2015) empirical models for a standard blind tee component and a sharp bend with a radius of 0.5 ID. The cavity depth of the blind tee empirical model is not defined explicitely in DNVGL-RP-O501 (2015) but is assumed to be greater than the flowpath ID. Two cases which are representative of single phase gas and liquid flow conditions with produced sand have been assessed.

CFD results for both production cases indicate that erosion results inside the "full" blind tee and sharp elbow (cavity depth of 0 ID) are in line with predictions from the empirical models. However, erosion rates inside the shallow blind tee with cavity depth of 0.38 ID are found to be one to two orders of magnitude greater than empirical model predictions using a short radius bend. An explanation for this behaviour is proposed based on the transient flow dynamics observed inside the cavity, both for the gas and liquid production cases.

These results should be confirmed by further numerical sensitivities and experimental evidence.

ACKNOWLEDGEMENTS

An important part of this work has been inspired by discussions with the DNVGL erosion modelling experts from Høvik, Norway. Their contribution is gratefully acknowledged.

REFERENCES

CHEN, X. *et al,* (2004), "Application and experimental validation of a computational fluid dynamics (CFD)-based erosion prediction model in elbows and plugged tees", *Computers & Fluids,* **33**, 1251-1272.

DNVGL-RP-O501, (2015), "Managing sand production and erosion".

LEONG M. and SANCHIS, A., (2016), "Intrusive erosion probes on subsea equipment – Design and placement considerations", *Offhore Technology Conference*, Kuala Lumpur, Malaysia, March 22-25.

SOMMERFELD M. *et al,* (2016), "Best practice guidelines for computational fluid dynamics of dispersed multiphase flows", *ERCOFTAC.*